Talanta 194 (2019) 585–590

Contents lists available at ScienceDirect

Talanta

journal homepage: www.elsevier.com/locate/talanta

pH sensing using whispering gallery modes of a silica hollow bottle resonator

Razvan-Ionut Stoian[a,1], Barry K. Lavine[b], A.T. Rosenberger[a,*]

[a] Department of Physics, Oklahoma State University, Stillwater, OK 74078, United States
[b] Department of Chemistry, Oklahoma State University, Stillwater, OK 74078, United States

ARTICLE INFO

Keywords:
PH sensor
Whispering gallery modes
Optical microresonator
Refractive index sensing
Swellable polymers
Hydrogels

ABSTRACT

The limitations of electrochemical pH sensors have stimulated the development of optical pH sensing methods. In the method reported here, swellable pH-sensitive polymer particles are deposited on the interior surface of a silica hollow bottle resonator. As the pH of the buffer solution in contact with the particles increases, the refractive index of the particles decreases. As a result, whispering gallery modes with internal evanescent components shift in frequency as a function of pH. This shift is monitored by the throughput of tunable diode laser light coupled into the whispering gallery modes using a tapered fiber. Plots of selected mode frequencies vs. pH yielded sigmoid shaped titration curves similar to those obtained using turbidity to monitor refractive index changes of the particles as a function of pH. The response time of 10–15 s and best resolution of 0.06 pH unit represent improvements over previous optical pH sensing methods.

1. Introduction

Optical pH sensors have attracted considerable attention, particularly in clinical, biomedical, and biotechnological analyses, as alternatives to well-established electrochemical methods, the use of which has proven to be problematic in many of these applications. Although electrochemical sensors (i.e., glass electrodes) are routinely used in laboratory settings, they are susceptible to changes in temperature and have a complicated readout scheme that is dependent on a reference electrode [1–3]. This, along with drift of the pH electrode and interference by other components, necessitates their continued recalibration. Furthermore, electrochemical sensors respond rather slowly and do not lend themselves well to miniaturization; all of these features limit their application to analysis problems in biological and environmental matrices. For these reasons, optical sensors are attractive. Two examples of optical methods of pH sensing include observing changes in near-infrared reflectance with varying pH [4,5] and measuring the pH-dependent modification of the absorption or fluorescence of an indicator dye in the visible or near-infrared region [6–10].

Herein, the focus will be on optical transduction methods that make use of swellable pH-sensitive polymers, which change their size as a function of the pH of the medium in contact with the polymer [11–15]. Along with structural modifications that occur within the polymer, optical constants such as its index of refraction also change, and sensing via the index change is a particularly attractive methodology because of the ease of refractive index measurement; it can be monitored in a variety of ways. Some of these refractive-index-change pH sensing methods involve absorbance measurements that are affected by the turbidity of a solution or membrane [12,13,16,17], surface plasmon resonance spectroscopy [18], observed frequency shifts in the transmission of a leaky coated fiber [10,19,20], and measurements of frequency shifts of the modes of a coated microresonator [21,22].

In this study, an optical pH sensor has been developed using swellable pH-sensitive hydrogel-embedded N–isopropylacrylamide (polyNIPA) particles [13,17] to functionalize the interior surface of a hollow bottle resonator (HBR) [23–27]. The focus of this work is pH sensing through frequency shift due to the change in the effective index of refraction measured by specific whispering gallery modes (WGMs) of the internally coated HBR. The WGMs whose frequencies shift are those with internal evanescent fields. Whispering gallery resonators have enabled numerous different sensing modalities [28–31], and hollow-core resonators such as the HBR permit internal sensing [28–30], as used here. The objective of this study is to demonstrate the utility and advantages of internal pH sensing using this scheme.

Previously published optical frequency-shift pH sensing, featuring the pH-sensitive polymers poly(allylamine hydrochloride) and poly (acrylic acid), was performed by recording either the throughput power loss due to the pH-dependent refractive index variation effects sensed

* Corresponding author.
E-mail address: atr@okstate.edu (A.T. Rosenberger).
[1] Present address: Department of Bioengineering, Rice University, MS-142, 6100 Main St., Houston, TX 77005, United States.

https://doi.org/10.1016/j.talanta.2018.10.077
Received 13 August 2018; Received in revised form 23 October 2018; Accepted 24 October 2018
Available online 27 October 2018
0039-9140/

by the external evanescent fields of a polymer-coated tapered fiber [10,19,20], or the shift of modes of a coated microresonator [21,22]. pH sensing was the focus in two cases [19,20], but was only tangential in the other three [10,21,22]. Compared to all of these frequency-shift sensing methods, our approach has several advantages with the potential to advance optical pH sensing, including simpler polymer deposition, smaller sample volume, faster response time, and better resolution owing to the use of high-quality-factor resonant WGMs.

2. Materials and methods

2.1. pH-sensitive polymer particles

pH-sensitive polyNIPA particles were prepared by photoinitiated dispersion polymerization using 14 mmoles of N-isopropylacrylamide (NIPA, transduction monomer), 2 mmoles of methacrylic acid (MAA, functional co-monomer), 2 mmoles of N-tertbutylacrylamide (NTBA), 2 mmoles of methylene bisacrylamide (MBA, crosslinker), and 100 mL of acetonitrile in a 500-mL three-neck round bottom Pyrex flask. The free radical photoreaction was performed at room temperature using 2, 2 dimethoxy-2-phenyl-acetophenone as the radical initiator in a Rayonet photoreactor (Southern New England Ultraviolet Company) equipped with G4T5 type mercury lamps (Atlanta Lightbulbs) and a cooling fan. Since the UV cutoff of the Pyrex flask is less than 260 nm, the monomer solution was radiated in the UV-A (315–400 nm) region. All chemicals were purchased from Aldrich (Milwaukee, WI) with the exception of NIPA and acetonitrile which were obtained from Acros (New Jersey, USA).

The polymer particles swell in response to an increase in the pH of the aqueous solution in contact with the polymer. At low pH, the polymer particles are in a shrunken state. When the pH of the aqueous solution is increased, a decrease occurs in the refractive index of the particles. This can be attributed to an increase in the water content of the particles due to swelling triggered by deprotonation of the pH-sensitive co-monomer. The particles go from a shrunken state to a swollen state in which their refractive index approaches that of the buffer solution in contact with the polymer. For polymer particles in solution, this leads to a decrease in the amount of light reflected by the particles. Thus the solution goes from turbid to clear in response to increasing pH (see Fig. 1) [17]. Fig. 1 also shows that swelling of the polyNIPA pH-sensitive polymer particles is affected by changes in the temperature of the buffer solution. In the work reported herein, the change in refractive index of a swellable polymer film is detected directly, complementing the turbidity measurement. The pH sensitive swellable NIPA polymer particles used in this study were selected

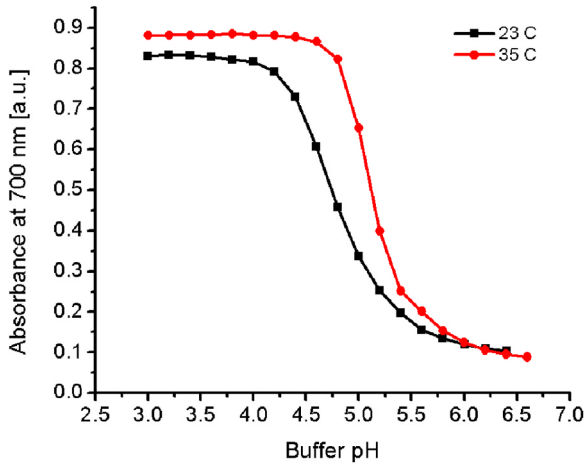

Fig. 1. Absorbance reduction due to swelling of poly NIPA particles in solution. pH response profile at 23°C and 35°C is shown (Adapted from Ref. [17]).

because of their unique properties which include large changes in the refractive index of the polymer particles in response to changes in the pH of the solution in contact with them, larger response over a narrower pH range than predicted by the Henderson-Hasselbach equation, swelling is both reversible and independent of the ionic strength of the solution as their ascending and descending pH profiles are superimposable, and the polymer can undergo multiple swelling and shrinking cycles without any loss of functionality [17].

The swelling of polymers containing ionizable functional groups has been described previously by Flory [32] via the expression

$$q_m^{5/3} = \left(\frac{V_0}{v_e}\right)\left[\left(\frac{1}{4}\right)\left(\frac{i}{V_u}\right)\left(\frac{1}{S^*}\right) + \frac{1/2 - \chi_1}{V_1}\right] \quad (1)$$

where q_m is the swelling ratio, V_0 is the volume of the unswollen polymer, v_e is the effective number of unit segments in the polymer network, i/V_u is the charge per network segment, S^* is the ionic strength, χ_1 is the polymer-solvent interaction parameter, and V_1 is the molar volume of the solvent in contact with the polymer. If the charge per polymer unit segment (i/V_u) is low, the effective charge density of the bulk polymer, which is $(V_0/v_e)(i/V_u)$, is also low, and the term $(1/2 - \chi_1)/ V_1$ predominates. Under these circumstances, swelling is independent of the ionic strength of the solution in contact with the polymer particles because swelling will be controlled by χ_1. The polymer-solvent interaction parameter of NIPA is larger in less polar solvents due to an incompatibility between the polymer and the solvent, which reduces the total swelling. χ_1 for NIPA will also increase with increasing temperature in water, leading to a volume phase transition that NIPA undergoes [33]. For the polyNIPA particles used in this study, swelling is nonionic because only a small amount of methacrylic acid is present in the formulation used to prepare the pH-sensitive polymer.

2.2. Experimental setup and procedure for pH sensing

The silica HBR was produced using a commercial silica capillary (Polymicro TSP700850) as the main building block. The silica capillary was etched using a solution of equal parts hydrofluoric acid (HF, aqueous, 48%) and methanol until its wall thickness was reduced from 50 ± 5 μm to 5–10 μm. (Care was taken to follow standard precautions for the safe handling of HF.) The bottle shape of this resonator was obtained by pressurizing the interior of the capillary and heating a 2–3 mm length of the capillary by applying an H_2/O_2 flame using a jeweler's torch until the diameter increased from 800 μm to 1000 μm in a symmetric bulge that provided axial mode confinement. This fabrication method is a simplified variation on earlier work [24–26] in that no arc discharge or CO_2 laser is required. Further details concerning the making of the HBR can be found elsewhere [27]. The interior surface of the HBR was coated by exposure to diluted polyNIPA solution (10 μL of the swellable polymer stock dispersion, 6.67% w/w, was diluted in 20 mL of methanol and the mixture was sonicated) for approximately 1.5–2 h.

Once the silica HBR was coated, it was introduced into a setup similar to the one used for chemical sensing with silica microspheres [34]. The HBR was coupled to a tapered optical fiber for excitation of WGMs, and buffer solutions of known pH were run into and out of the HBR. Variations in WGM resonant frequencies were recorded and processed as described below. The experimental setup is depicted in Fig. 2.

Light from a tunable diode laser (New Focus TLB-6330, wavelength ~ 1580 nm, linewidth < 300 kHz), frequency scanned by a (Tektronix CFG253) function generator, is injected into a single mode fiber (SMF28) tapered down to approximately 2 μm in diameter. Before the light is coupled to the HBR, the fiber is run through a linear polarization controller that helps select specific polarizations for the WGMs. The signal is extracted by the same tapered fiber and fed into a detector

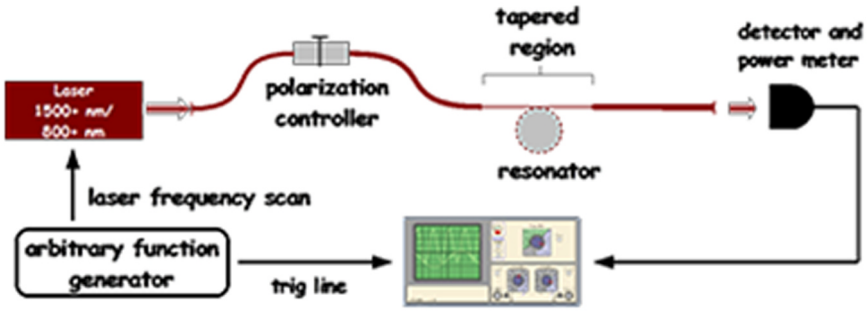

Fig. 2. Simplified schematic of the frequency shift experiment.

(Newport 818-IR), which measures a dip in the throughput power when the laser scans through each WGM's resonance frequency. The power meter (Newport 2832-C) attached to the detector is coupled to an oscilloscope (Tektronix TDS 420 A) which records the throughput spectrum resulting from the laser frequency scan.

Careful attention was given to the positioning of the resonator with respect to the tapered fiber. To keep the analyte immobile during data collection, the HBR was oriented horizontally, and so the tapered fiber was mounted vertically, at 90° to the resonator, as shown in Fig. 3. The tapered coupling fiber could be placed in the HBR's equatorial plane, i.e., centered on the bulge in the capillary, or could be offset from center but kept parallel to the equatorial plane.

The two vertical arrows in Fig. 3 indicate the propagation direction of light in the tapered coupling fiber and the horizontal arrow indicates the direction in which the buffer solution flows into the HBR. The introduction of the buffer solution in the system was handled as follows. The extremities of the capillary with the resonator bulge were epoxied to a pair of 5-cm-long smaller diameter capillaries. Their ends were epoxied to two capped plastic vials, one used as the main reservoir for the buffer solution and the other with a plastic syringe attached to force the buffer through the capillary. The two plastic vials were tightly mounted and secured using metallic mounts screwed into the optical table and, with the speed of buffer replenishment slow enough, vibration of the apparatus was minimized.

Buffer solutions were prepared using either chloroacetic acid (pH 3-pH 3.8) or acetic acid (pH 3.9-pH 5.4). To prepare buffer solutions of fixed ionic strength (0.1 M), a known amount of NaCl was added to each buffer solution. An online buffer calculator (www.liv.ac.uk/buffers/buffercalc.html) was used to determine the composition of each buffer for a specific pH and fixed ionic strength. The precision in the pH values of the buffers is approximately 0.02 pH units. Buffers of pH which varied in steps of 0.2 were introduced in the capillary as follows. 200 µL of buffer solution was placed in the first plastic vial. Using a syringe feed, a small volume of the buffer solution was run though the capillary. After the data recording using the setup of Fig. 2 was completed, the entire buffer solution was pushed back into the first container and discarded. A new buffer solution of different pH was then introduced into the system using this procedure and after the system stabilized (about 15 s) new waveforms were recorded for further processing.

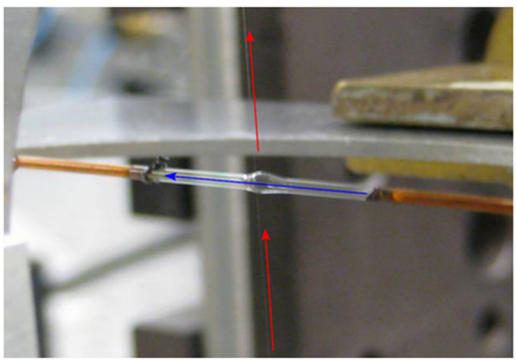

Fig. 3. The relative position of the fiber with respect to the resonator. Vertical arrows show direction of light propagation in tapered fiber and horizontal arrow shows flow direction of buffer solution introduced into HBR.

2.3. Sensing

The pH value of a buffer solution in contact with the polymer is sensed through the variation of the polymer's refractive index (~ 1.32). This change in index of refraction of the polymer causes a change of the effective refractive index (n_{eff} ~ 1.40) for the WGM whose frequency is shifted. Assuming that the thickness of the polymer film (~ 1 µm) is greater than the decay length of the evanescent field (~ 0.44 µm), the change in the effective refractive index is equal to the internal evanescent fraction, f (~ 3%), times the change in polymer index, and so the frequency shift $\Delta\nu_{WGM}$ is given by

$$\frac{\Delta\nu_{WGM}}{\nu} = -f\frac{\Delta n_{polymer}}{n_{eff}} \quad (2)$$

The HBR's throughput power spectrum could be monitored while the interior surface was being coated with polyNIPA. A decrease by an order of magnitude of the Q (quality factor, inversely proportional to the width of the resonance dip in the throughput power spectrum) of certain WGMs (those of higher radial order, with appreciable internal evanescent fractions) was a clear indication that a thin film was successfully deposited on the inner surface of the resonator. For the results shown in Fig. 4, a small volume of the diluted polymer dispersion was introduced into the HBR and left to deposit in the form of a film on the inner walls of the resonator. The deposition process took approximately 1.75 h to complete. Fig. 4 shows the real-time monitoring of the polymer deposition by following the frequency redshifts of selected WGMs as the surface coverage of the deposited film, which has an index of refraction greater than that of the polymer solution, increased. Note that the WGM located at approximately 9.5 GHz does not shift, because it has no internal evanescent fraction owing to its low radial order; such modes serve as frequency references.

3. Results and discussion

Frequency shift experiments were performed at room temperature (~ 23 °C) using HBRs coated with polyNIPA-MAA. Results are reported for internal coating, using two different positions of the coupling fiber, and also for external coating. In a typical frequency shift experiment, the wavelength of the frequency-scanned (over an 18 GHz range) diode laser was set at 1580.6 nm. The time taken for a full-range scan was 20 ms, and the throughput power collected at the end of the tapered fiber was 14 µW. For the results shown in Fig. 5, the tapered-fiber coupler was centered on the HBR, i.e., in its equatorial plane. The measuring method for frequency shift as a function of pH involved a two-step approach. First, a WGM having a negligible internal

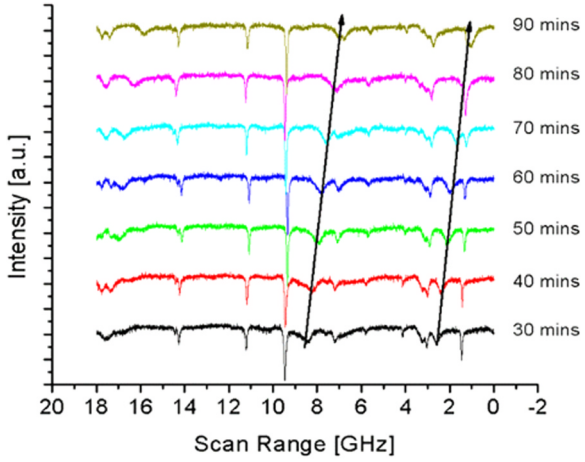

Fig. 4. Real-time monitoring of the polymer deposition using frequency shifts. Relative frequency scans of WGM throughput power spectra, beginning 30 min after introducing the polymer solution, are taken at 10-min intervals, and successively displaced upward in the figure. The arrows emphasize the shifts of two WGMs that have internal evanescent fractions. The WGM at 9.5 GHz has no internal evanescent fraction, because it is a mode of low radial order, so it does not shift during the deposition process.

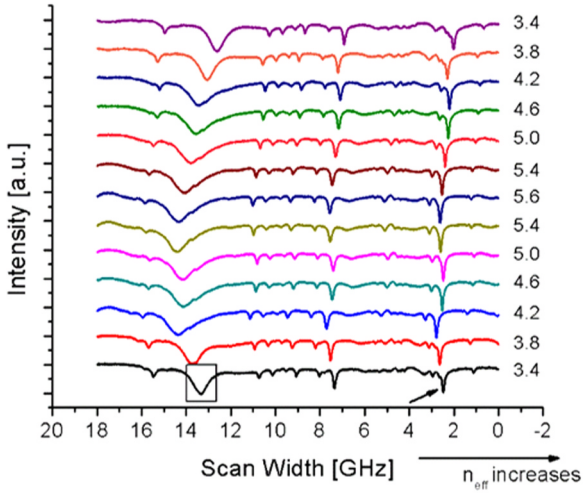

Fig. 5. WGM frequency shifts due to pH variation. The arrow indicates the WGM chosen as a reference for frequency shift measurement of the boxed WGM. The boxed WGM is affected by the swelling of the polyNIPA-MAA particles. Each successive trace is displaced upward as the pH is increased from 3.4 to 5.6 and then decreased back to 3.4.

evanescent fraction to interact with the polyNIPA-MAA particles was identified; this WGM's frequency would not shift with increasing pH and the WGM is indicated by a small arrow in Fig. 5. Hence, this WGM was used as a measurement reference for the observed frequency shifts of the WGM boxed in Fig. 5. Once the frequency shifts were recorded, the normalized frequency shift for each pH was found by measuring the difference in frequency between the pH-shifted mode (boxed in Fig. 5) and the reference mode (arrow in Fig. 5), and then subtracting the initial pH-3.4 frequency difference which served as the reference for all measurements. This assigns an initial normalized frequency shift of 0 at pH 3.4. Having a reference WGM whose frequency is unaffected by the change in pH offers an advantage regarding data collection because frequency drifts such as those due to thermal effects (–1.6 GHz/K) are common-mode rejected.

Note that the shape of the throughput dip of the shifted WGM changes as it blueshifts with increasing pH. It becomes shallower, broader, and asymmetric. These changes result from two different but

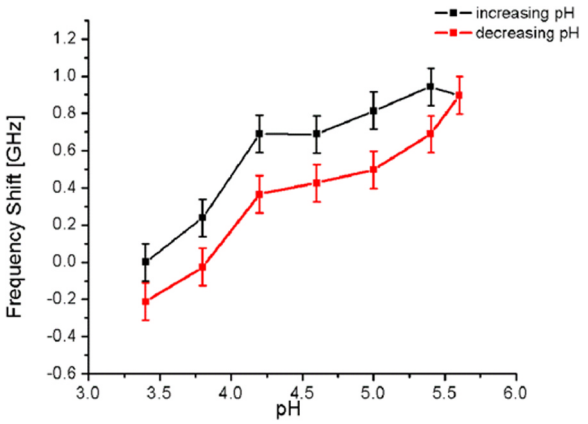

Fig. 6. Normalized frequency shifts (from Fig. 5, centered coupling fiber) relative to that at the initial pH of 3.4, showing hysteresis. The error bars reflect the estimated uncertainty in determining the position of the lower-*Q* shifted WGM.

simultaneous effects. First, the optical absorption and scattering of polyNIPA decrease with increasing pH, changing the total WGM loss and the ratio of output coupling loss to total loss. This will affect the depth and width of the dip. Second, another lower-*Q* WGM may be present, initially at the same frequency as the sensing WGM, but shifting less. This leads to asymmetry and affects the apparent width of the dip. Such mode overlap can limit the precision of measurements of the frequency shift of the sensing WGM. Absorption due to the polymer coating and the buffer solution could provide another method of sensing changes in pH [27], but it does not affect the frequency shift. In this work, only the frequency shift with changing pH is studied.

The normalized frequency shifts of the WGM of interest as a function of pH of the buffer solution in the resonator are shown in Fig. 6. The hysteresis feature of the data in Fig. 6 indicates that once the polymer particles are fully swollen, and the pH of the buffer solution is then decreased, the polymer does not return to its initial state; it appears to shrink by a larger amount when the pH of the buffer solution is returned to 3.4. This hysteresis is related to the volume phase transition mentioned earlier [33]. The hysteresis in one sensing cycle of increasing and decreasing pH can be reduced by repeating for several cycles [15,17]. For this particular position of the tapered fiber (centered on the HBR), the strong overlap of the low-*Q* modes limited the measurement precision of the frequency shift.

Therefore, an additional experiment was performed on the system with the tapered fiber placed in an offset position relative to the center of the HBR. This facilitates the selection of an isolated low-*Q* WGM, since offsetting the coupling fiber reduces the WGM spectral density. In this case, overlap of lower-*Q* (higher radial order) WGMs was noticeably reduced. There was still some overlap of the lower-*Q* sensing WGM with a narrower higher-*Q* WGM, but this does not affect the frequency shift measurement precision as strongly. For this offset position of the coupling fiber, normalized WGM frequency shifts are shown in Fig. 7.

The results of the two experiments (Figs. 6 and 7) are consistent, indicating a WGM shift toward higher frequencies or smaller n_{eff} with increasing pH. Moreover, the curve corresponding to decreasing pH in Fig. 7 shows that when the pH of the buffer solution is brought back to 3.4, the frequency shift is again negative (-0.12 GHz) relative to the initial measurement, but the overall hysteresis is less. As in the case for the initial experiment (Fig. 6), there is a slight decrease in the frequency shift at pH 5.6. This indicates that the polymer becomes saturated in the vicinity of pH 5.5. The most dramatic frequency shifts happen in both cases between pH 3.8 and pH 4.2 and are, respectively, 0.44 GHz in Fig. 6 and 0.62 GHz in Fig. 7.

Only a lower limit for the variation of the refractive index of the polymer particles could be estimated, because the WGM frequency shift

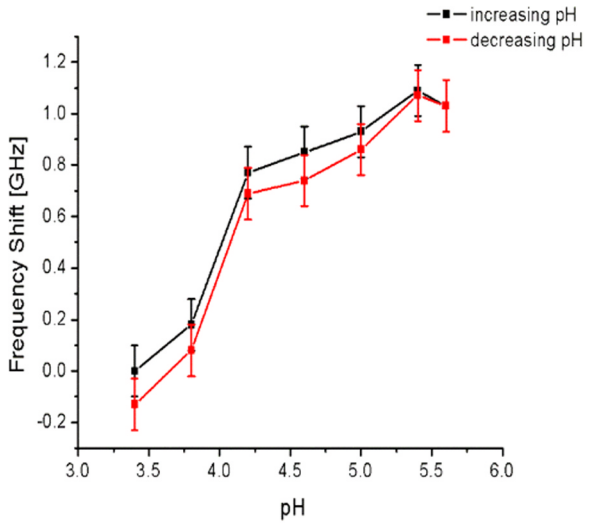

Fig. 7. Normalized frequency shifts (coupling fiber offset from center) relative to that at the initial pH of 3.4.

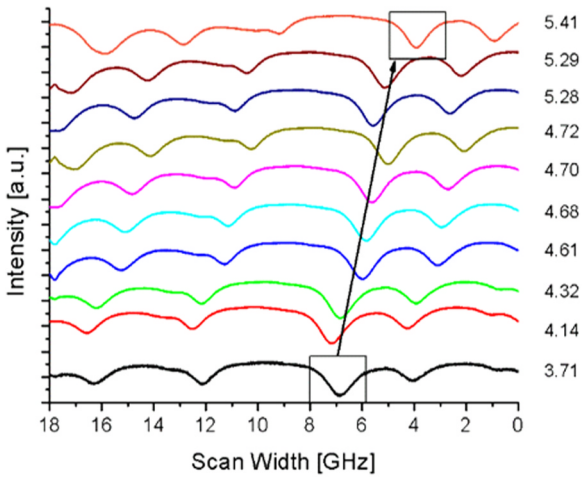

Fig. 8. WGM frequency shift with increasing pH in a polymer-coated bottle resonator in external sensing configuration. Each step in pH resulted from adding NaOH and allowing the solution to equilibrate for about 2 h. The arrow indicates the shift of the boxed WGM, perturbed by temperature fluctuations.

results from two opposing effects, the variation in the refractive index of the particles and the variation in the refractive index of the buffer solution. As will be shown in the external-coating experiment to be described later, the latter always shows an increase in refractive index with increasing pH. It might contribute because, although the polymer particles have diameters of approximately 1 μm, more than twice the evanescent field decay length, the coating may have contained interstices in which the WGM's evanescent field could interact with the buffer. Using Eq. (2), the maximum shift from Fig. 7, and assuming an internal evanescent fraction $f = 0.03$, slightly larger than the external evanescent fraction observed earlier for immersed microspheres [34], we find that $\Delta n_{polymer} \approx 3 \times 10^{-4}$. The smaller frequency shift seen in Fig. 6 could be due to the polymer coating being sparser, the WGM's evanescent fraction, f, being smaller, or both.

These WGM shifts, in wavelength, are about 33 nm/RIU (refractive index unit of the polymer), as seen from the 1.2 GHz shift in Fig. 7 for the estimated index change of 3×10^{-4}. This wavelength shift, typical for evanescent sensing, indicates that the estimated value of f is reasonable. In comparison to the coated-fiber results mentioned earlier [10,19,20], the method described here shows an improved speed of response and at least equivalent resolution. The response time, which is at most 10–15 s, is predominantly due to stabilization after introducing new buffer, and is about five times faster than the response reported in Ref. 20. The resolution is $\pm \sim 0.06 - 0.20$ pH unit, depending on which portion of Fig. 7 is used for the estimation, the lower limit for the steepest part of the curve and the upper limit for the average slope; the error bars in Fig. 7 were conservatively large; hence, the actual resolution may be better. The coated-resonator methods [21,22] had even slower response times and poorer resolution, likely due to their use of an external coating. As discussed below, internal sensing gives better results than external sensing.

The experiments described thus far were performed using the internal sensing method, which ensures that the external surface of the resonator is not affected by the polymer film or the buffer solution. In order to emphasize the importance of this method over external sensing, the exterior of the HBR was dipped into the diluted swellable polymer dispersion (polyNIPA-MAA) for approximately 1 h. Once coated, the bottle resonator was suspended vertically, brought into contact with the tapered fiber, and the entire ensemble immersed into a small container filled with 100 mL of pH 3.4 buffer solution. The gradual pH increase of the initial buffer solution was performed by adding increments of 1 mL of NaOH (0.1 M) and monitoring the pH in real time using a pH meter. This method was particularly tedious since diffusion and pH stabilization times varied widely, from 1 to 3 h. Another drawback of the external sensing approach was the irreversible contamination of the tapered fiber (resulting in a 90% drop in throughput power) immediately after the exposure to buffer solution. A third drawback of external coating was that it was not possible to excite WGMs that could have been used as unshifted references for the polymer-mediated-frequency-shifted WGMs. Fig. 8 shows a set of WGMs collected over the course of several hours, as the pH of the buffer solution was slowly increased.

As shown in Fig. 8 for the external sensing configuration, the frequency shifts were not indicative of polymer swelling, but rather were dominated by the increase in the refractive index of the buffer solution with increasing pH and the varying temperature of the buffer solution. In order to make the swellable polymer-mediated technique viable for external sensing, the concentration of polymer particles would have to be increased by nearly an order of magnitude. However, this would render the resonator unusable because the resonator-taper coupling would be adversely affected due to the increased thickness of the polymer film.

4. Conclusions

In the preliminary work presented in this study, pH sensing is shown to be another interesting application of silica HBRs. A deposition method for swellable pH-sensitive polymer particles (polyNIPA-MAA) on the inner surface of the HBR was successfully developed, and the frequency shifts of WGMs with internal evanescent fractions were used to sense the polyNIPA's refractive index change with varying pH. One of the most important outcomes of this experiment is the demonstration that internal coating is the only viable sensing approach, since attaching the polymer to the resonator's external surface rendered the HBR unusable as a sensor. Moreover, internal sensing is advantageous because WGMs with negligible internal evanescent fractions can be used as frequency references, eliminating the adverse effects of other causes of frequency shifts such as temperature variation.

An improvement to our method would result from the selection of WGMs that do not exhibit strong frequency overlapping. As observed here, modal overlap increases the difficulty of reading the frequency shifts due to pH variation. The use of an offset of the coupling fiber from HBR center (by even more than in the second experiment above) and/or a larger-diameter coupling fiber can help to reduce the mode density and resulting overlap. Using HBRs with even thinner walls would also help in this regard.

A drawback of our method compared to pH sensors based on molecular coatings such as bovine serum albumin (BSA) is the large size of the polyNIPA particles [21]. Since thin-film-related theoretical models [21] do not apply in the case of the (larger) polyNIPA particles, it is difficult to make a good estimate of the absolute variation of the refractive index of the polymer film, as this depends on the value of *f*. Therefore, the use of alternative pH-sensing agents that can be incorporated into films thin compared to the internal evanescent decay length is highly recommended. Alternatively, a method [34] for measuring *f* could be further developed and made more reliable.

A future experiment involving this type of resonator used in conjunction with this class of polymers would involve coating the interior walls of the HBR with molecularly-imprinted polyNIPA particles [18]. The main advantage of using these particles is their response to specific organic analytes. In other words, the HBR can be used as a sensor for selected organic compounds regardless of their optical absorption properties above or below 1550 nm. In addition, since the initial absorption experiments featuring polyNIPA particles were performed at around 700 nm (as shown in Fig. 1), it is obvious that the WGM-based experiments described earlier can be easily carried out in the near infrared as well as at telecom wavelengths. This would have the advantage of better resolution, resulting from the higher WGM quality factors due to decreased absorption in the polymer.

In recent years, measuring pH in the ocean has become important because of rising acidity levels due to the water becoming enriched in carbon dioxide (and in turn) reducing the amount of carbonate available for shell building organisms [35]. The silica hollow bottle resonator described in this study could serve as a sensor platform to monitor pH in ocean waters provided that a suitable pH sensitive polymer is incorporated into the platform and visible or near-infrared light is used to minimize absorption and provide high WGM quality factors.

Acknowledgment

The authors acknowledge the assistance of Undugodage Perera and Sandhya Pampati for the preparation of polyNIPA dispersions and the buffer solutions used in this study. BKL acknowledges the financial support of the Environmental Protection Agency through Science to Achieve Results (STAR) RD-830911101-0.

References

[1] E. Bakker, M. Telting-Diaz, Electrochemical sensors, Anal. Chem. 74 (2002) 2781–2800.
[2] W. Vonau, U. Guth, pH monitoring: a review, J. Solid State Electrochem. 10 (2006) 746–752.
[3] U. Guth, W. Vonau, J. Zosel, Recent developments in electrochemical sensor application and technology – a review, Meas. Sci. Technol. 20 (2009) 042002.
[4] M.K. Alam, J.E. Franke, T.M. Niemczyk, J.D. Maynard, M.R. Rohrscheib, M.R. Robinson, R.P. Eaton, Characterization of pH variation in lysed blood by near-infrared spectroscopy, Appl. Spectrosc. 52 (1998) 393–399.
[5] S. Zhang, B.R. Soller, R.H. Micheels, Partial least-squares modeling of near-infrared reflectance data for noninvasive in vivo determination of deep-tissue pH, Appl. Spectrosc. 52 (1998) 400–406.
[6] E.J. Netto, J.I. Peterson, M. McShane, V. Hampshire, A fiber-optic broad-range pH sensor system for gastric measurements, Sens. Actuat. B 29 (1995) 157–163.
[7] J.A. Ferguson, B.G. Healey, K.S. Bronk, S.M. Barnard, D.R. Walt, Simultaneous monitoring of pH, CO_2 and O2 using an optical imaging fiber, Anal. Chim. Acta 340 (1997) 123–131.
[8] A.S. Jeevarajan, S. Vani, T.D. Taylor, M.M. Anderson, Continuous pH Monitoring in a Perfused Bioreactor System Using an Optical pH Sensor, Biotech. Bioeng. 78 (2002) 467–472.
[9] M. Mosshammer, M. Strobl, M. Kühl, I. Klimant, S.M. Borisov, K. Koren, Design and Application of an Optical sensor for Simultaneous Imaging of pH and Dissolved O_2 with low cross-talk, ACS Sens. 1 (2016) 681–687.
[10] R. Gupta, N.J. Goddard, Broadband absorption spectroscopy for rapid pH measurement in small volumes using an integrated porous waveguide, Analyst 142 (2017) 169–176.
[11] J. Dübendorfer, R.E. Kunz, G. Jobst, I. Moser, G. Urban, Integrated optical pH sensor using replicated chirped grating coupler sensor chips, Sens. Actuat. B 50 (1998) 210–219.
[12] M.T.V. Rooney, W.R. Seitz, An optically sensitive membrane for pH based on swellable polymer microspheres in a hydrogel, Anal. Commun. 36 (1999) 267–270.
[13] B.K. Lavine, D.J. Westover, N. Kaval, L. Oxenford, New approaches to chemical sensing-sensors based on polymer swelling, Anal. Lett. 39 (2006) 1773–1783.
[14] O. Korostynska, K. Arshak, E. Gill, A. Arshak, Review on state-of-the-art in polymer based pH, Sensors, Sensors 7 (2007) 3027–3042.
[15] A. Richter, G. Paschew, S. Klatt, J. Lienig, K.-F. Arndt, H.-J.P. Adler, Review on hydrogel-based pH sensors and microsensors, Sensors 8 (2008) 561–581.
[16] D.J. Westover, B.K. Lavine, W.R. Seitz, Synthesis and evaluation of nitrated poly(4-hydroxystyrene) microspheres for pH sensing, Microchem. J. 74 (2003) 121–129.
[17] B.K. Lavine, L. Oxenford, M. Kim, N. Kaval, M. Benjamin, W.R. Seitz, Novel turbidimetric method to study polymer swelling, Microchem. J. 103 (2012) 97–104.
[18] B.K. Lavine, G. Mwangi, N. Mirjankar, M. Kim, Characterization of swellable molecularly imprinted polymer particles by surface plasmon resonance spectroscopy, Appl. Spectrosc. 66 (2012) 440–446.
[19] B. Gu, M.-J. Yin, A.P. Zhang, J.-W. Qian, S. He, Low-cost high-performance fiber-optic pH sensor based on thin-core fiber modal interferometer, Opt. Express 17 (2009) 22296–22302.
[20] A.B. Socorro, I. Del Villar, J.M. Corres, F.J. Arregui, I.R. Matias, Tapered single-mode optical fiber pH sensor based on lossy mode resonances generated by a polymeric thin-film, IEEE Sens. J. 12 (2012) 2598–2603.
[21] J.-W. Hoste, S. Werquin, T. Claes, P. Bienstman, Conformational analysis of proteins with a dual polarisation silicon microring, Opt. Express 22 (2014) 2807–2820.
[22] J. Nishimura, M. Kobayashi, R. Saito, T. Tanabe, NaCl ion detection using a silica toroid microcavity, Appl. Opt. 54 (2015) 6391–6396.
[23] X. Fan, I.M. White, H. Zhu, J.D. Suter, H. Oveys, Overview of novel integrated optical ring resonator bio/chemical sensors, Proc. SPIE 6452 (2007) 64520M.
[24] M. Sumetsky, Y. Dulashko, R.S. Windeler, Optical microbubble resonator, Opt. Lett. 35 (2010) 1866–1868.
[25] M. Sumetsky, Y. Dulashko, R.S. Windeler, Super free spectral range tunable optical microbubble resonator, Opt. Lett. 35 (2010) 898–900.
[26] G.S. Murugan, M.N. Petrovich, Y. Jung, J.S. Wilkinson, M.N. Zervas, Hollow-bottle optical microresonators, Opt. Express 19 (2011) 20773–20784.
[27] R.I. Stoian, K.V. Bui, A.T. Rosenberger, Silica hollow bottle resonators for use as whispering gallery mode based chemical sensors, J. Opt. 17 (2015) 125011.
[28] J. Wang, T. Zhan, G. Huang, P.K. Chu, Y. Mei, Optical microcavities with tubular geometry: properties and applications, Laser Photonics Rev. 8 (2014) 521–547.
[29] Y. Yang, J. Ward, S. Nic Chormaic, Quasi-droplet microbubbles for high resolution sensing applications, Opt. Express 22 (2014) 6881–6898.
[30] J.M. Ward, N. Dhasmana, S. Nic Chormaic, Hollow core, whispering gallery resonator sensors, Eur. Phys. J. Spec. Top. 223 (2014) 1917–1935.
[31] M.R. Foreman, J.D. Swaim, F. Vollmer, Whispering gallery mode sensors, Adv. Opt. Photon. 7 (2015) 168–240.
[32] P.J. Flory, Principles of Polymer Chemistry, Cornell University Press, Ithaca, 1953.
[33] H.G. Schild, Poly(N-isopropylacrylamide): experiment, theory, and application, Prog. Polym. Sci. 17 (1992) 163–249.
[34] G. Farca, S.I. Shopova, A.T. Rosenberger, Intracavity chemical absorption sensing using microresonator whispering-gallery modes, Proc. SPIE 5855 (2005) 427–430.
[35] R.F. Service, Rising acidity brings an ocean of trouble, Science 337 (2012) 146–148.